Journal of Physics D: Applied Physics

PAPER • **OPEN ACCESS**

Electrically-driven IMT and volatile memristor behavior in $NdNiO_3$ films

To cite this article: O D Schneble *et al* 2024 *J. Phys. D: Appl. Phys.* **57** 485301

OPEN ACCESS
IOP Publishing
Journal of Physics D: Applied Physics
J. Phys. D: Appl. Phys. **57** (2024) 485301 (6pp)
https://doi.org/10.1088/1361-6463/ad714e

Electrically-driven IMT and volatile memristor behavior in $NdNiO_3$ films

O D Schneble[1,2], I A Leahy[2], J D Zimmerman[1,2] and M B Tellekamp[2,*]

[1] Department of Physics, Colorado School of Mines, Golden, CO, United States of America
[2] National Renewable Energy Laboratory, Golden, CO, United States of America

E-mail: brooks.tellekamp@nrel.gov

Received 3 May 2024, revised 10 July 2024
Accepted for publication 20 August 2024
Published 4 September 2024

Abstract

Transition metal oxides with insulator-metal transitions (IMTs) are uniquely suited for volatile memristor devices that mimic the spiking of biological neurons. Unlike most non-volatile memristors, which often operate via ion migration into filaments, volatile devices utilize a reversible phase change that returns to a ground state in the absence of applied stimulus. In these devices, Joule heating triggers the IMT and changes the bulk resistivity rather than influencing conduction through defects, as in previous studies. This volatile resistive switching behavior has previous been leveraged in niobium and vanadium oxides, but not in rare-earth nickelates, despite their tunable transition temperatures. This study demonstrates an electrically driven IMT in the prototypical rare-earth nickelate, $NdNiO_3$, in large area devices. While previous work examining the electrically-driven IMT in $NdNiO_3$ suggests defect-dominated conduction, this study shows clear s-type negative differential resistance (NDR) consistent with temperature-dependent resistivity measurements. The NDR peak-to-valley voltage scales linearly with temperature as expected for conductivity pathways dominated by bulk IMT behavior. Unlike other transition metal oxides, which are modeled using the insulator-metal phase fraction as the internal state variable, a thermoelectric model with temperature as the internal state variable is found to more accurately describe the current–voltage characteristic of $NdNiO_3$ volatile memristors. Overall, we report the synthesis, fabrication, and characterization of $NdNiO_3$ volatile memristors with resistivity dominated by bulk-like IMT behavior which is scalable and not dependent upon oxygen vacancy migration or defect mediated conduction pathways.

Supplementary material for this article is available online

Keywords: neuromorphic, volatile memristor, rare-earth nickelate, epitaxial thin film, memristive device

1. Introduction

Materials with temperature-driven insulator-metal transitions (IMTs), such as vanadium oxides, niobates, and rare-earth nickelates, have garnered interest for their applications to resistive switching devices, particularly volatile memristors that mimic biological neurons [2]. In this context, the IMT can be driven electrically by Joule heating and is reversed when electrical input is removed and the material passively cools. Volatile memristors have been demonstrated with VO_2 and NbO_2, which have IMT temperatures at roughly 340 K and 1100 K, respectively. Rare-earth nickelates ($RNiO_3$, where R = rare-earth) have IMTs spanning a wide range of temperatures (100–600 K) and can be alloyed to achieve intermediate properties, making them interesting for volatile memristors

* Author to whom any correspondence should be addressed.

operating at typical microprocessor temperatures (350–450 K) with potentially tunable properties [6]. This work examines the applicability of $R\mathrm{NiO_3}$ thin films as volatile memristor devices.

The IMTs of transition metal oxides are phase changes in which small shifts in lattice or electronic symmetry strongly impact the electronic behavior. These structural changes are subtle and reversible, which differentiates them from many memristor materials that depend on ionic motion or filament formation [17]. In the latter case, changes tend to persist in the absence of electronic stimulus, which can be leveraged for some nonvolatile memristive applications, but can also shorten device lifetimes. Defect-mediated conduction also calls into question the scalability of these devices, which would be constructed into large arrays of sub-μm devices in a large artificial neural network application [19]. In electrical measurements, $\mathrm{NbO_2}$ also displays an abrupt increase in conductivity due to a Poole–Frenkel electron hopping mechanism with heating to 400–500 K [12]. Unlike the IMT phase transition, Poole–Frenkel conduction relies on traps, specifically oxygen vacancies, which can migrate through the material and limit the lifetime and reliability of $\mathrm{NbO_2}$ devices. In addition, $\mathrm{NbO_2}$ devices are often individually electroformed before they show the desired electrical behavior—an operation that cannot be scaled to required device densities [13, 14]. Similarly, in the few studies of volatile resistive switching in $R\mathrm{NiO_3}$, the current-driven V–I measurements have discontinuities that are not fully explained by the resistivity drop of the IMT [4, 7]. Implementing such neuron-inspired devices requires a scalable and robust mechanism that can be fabricated in large arrays.

Modeling the electrical behavior of these devices is also an important step towards such practical applications. Previous work has used mathematical models of the underlying physics implemented in LTspice to simulate artificial neuron dynamics in $\mathrm{VO_2}$ and $\mathrm{NbO_2}$ [14–16, 19]. Most studies of $\mathrm{VO_2}$ and $\mathrm{NbO_2}$ volatile memristors have used a model proposed by Pickett *et al*, which assumes the insulating phase and conducting phase have constant, temperature-independent properties and allows them to vary in proportion so the device conductivity varies in response to resistive heating. This scheme will be called the 'phase fraction model.' Another model, called 'thermoelectric' by Brown *et al*, describes the resistance as a function of the average device temperature [3]. Both models use heat capacity, thermal conductivity, and other material parameters to relate power dissipation and device temperature, and both make significant assumptions of homogeneity.

In this work, lateral devices are fabricated without electroforming from epitaxial $\mathrm{NdNiO_3}$ films and demonstrate electrically-driven IMT consistent with the temperature-driven IMT measured across the films. The phase fraction and thermoelectric models are evaluated and the thermoelectric model is found to be better-suited to $R\mathrm{NiO_3}$ devices.

2. Experimental

Epitaxially-oriented thin films of $\mathrm{NdNiO_3}$ were grown on a single-crystal (001) $\mathrm{NdGaO_3}$ substrate (Shinkosha Co., Ltd.) by off-axis RF magnetron sputtering with a target to substrate angle of 65°. The resistive substrate heater was set to 450 °C, and a working pressure of 50 mTorr was maintained for all growths. The first sample received Ar and $\mathrm{O_2}$ gases in a 7:2 ratio with a cathode power of 50 W, while the second sample received Ar and $\mathrm{O_2}$ in a 7:3 ratio with a cathode power of 30 W.

X-ray diffraction (XRD) characterization was performed using a Rigaku SmartLab diffractometer with a Cu-Kα beam monochromated by a 2-bounce (220) Ge channel cut crystal. The resulting Pendellösung fringes were used to estimate film thickness: both approximately 10 nm. Electrical measurements were performed in a Quantum Design physical property measurement system (PPMS) on two different sample holders: a plastic 14-pin chip holder that fits in a custom epoxy puck, termed 'chip holder,' and a metal pucks provided by Quantum Design for dc resistance measurements, termed 'resistivity puck.' First, Ni/Au (10 nm/100 nm) contacts 3–5 mm in diameter were deposited with a spacing of 5 mm such that they meet the sample edges. Due to concerns about film stability, contacts were not annealed. Both samples were placed on chip holders for sheet resistance measurements in four-probe Van der Pauw configuration. Next, additional contacts with a 500 μm diameter were deposited in the middle of the sample, approximately 1 mm away from the previous contacts (figure 1(c)). Then the 50 W sample was placed back on a chip holder and the 30 W sample was placed on a resistivity puck for lateral 2-probe device measurements.

3. Results

The two samples used in this study, each about 10 nm thick, had slightly different out-of-plane lattice constants, apparent in the symmetric XRD scans of the (004) reflections (figure 1(a)). The samples also had different absolute resistivities, but similar relative changes in resistivity ($\Delta R/R$) and transition temperatures (T_{IMT}) (figure 1(b)). The slight difference in out-of-plane lattice constant between the two films may describe different strain states or different populations of oxygen vacancies, which are known to expand the lattice in oxides [10, 11]. The reciprocal space map of the (026) reflection of the 30 W sample, inset, suggests the films are fully strained to the substrate.

Two-terminal lateral electrical measurements were first performed on the 30 W sample on the plastic chip holder. In current-controlled V–I sweeps, taken at 75 K, the sample on the plastic chip holder displayed the expected negative differential resistance (NDR) as well as an unexpected hysteresis loop (figure 2(a)). The hysteresis loop under voltage-controlled measurements is expected for this type of volatile memristor, but the hysteresis in current-control indicates that the device is not at steady state. The data in (a) and (c) show time evolution, indicated by the data point color, at each current or voltage step. Further measurements taken on this sample at 50 K show symmetric NDR and calculated resistance under opposite polarities of applied current (figures 2(b) and (d)). The data points in (b) and (d) are averaged for each step in current.

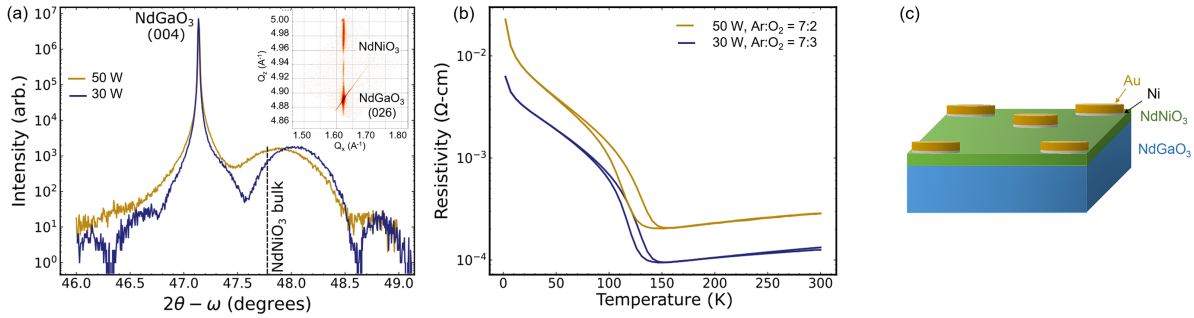

Figure 1. (a) Symmetric x-ray diffraction $\omega - 2\theta$ scans around the substrate (004) reflection; the dashed line indicates the expected position of the bulk $NdNiO_3$ (004) reflection, showing the films are in tensile strain. An RSM of the 30 W sample, inset, indicates in-plane strain to the substrate. (b) Resistivity vs. temperature measured by four-probe method, and (c) schematic of one of the samples with contacts for lateral devices.

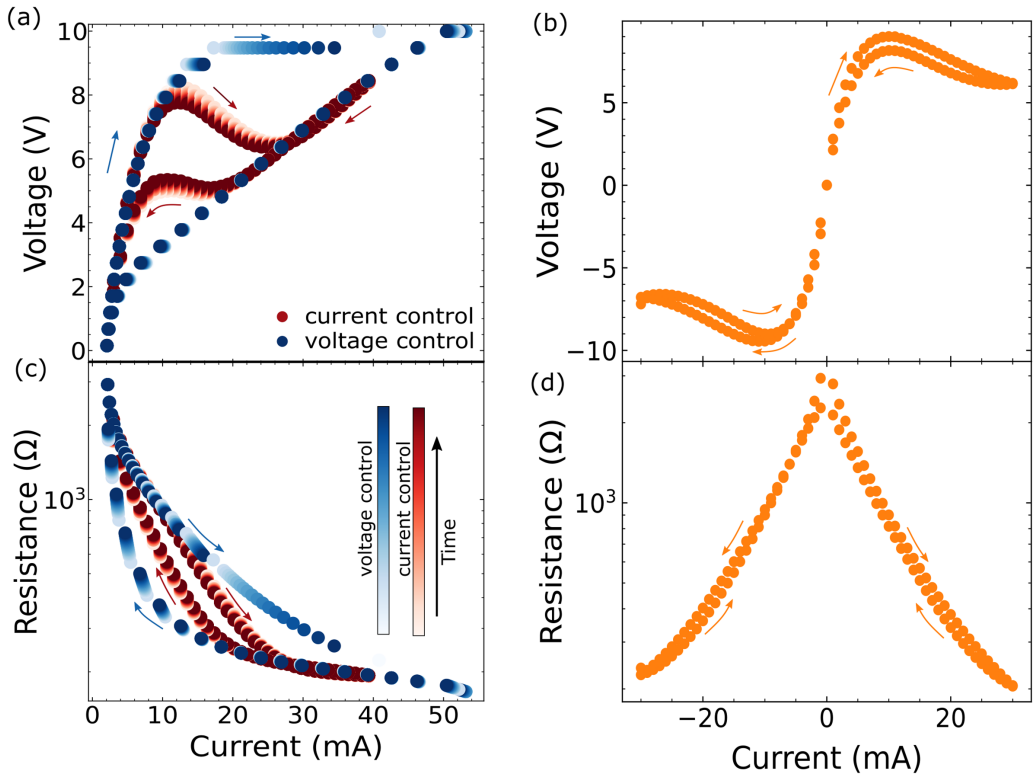

Figure 2. Resistivity measurements of a sample mounted on the plastic chip holder. (a) Current-controlled V–I measurement and voltage-controlled I–V measurement at 75 K with 20 data points per step showing time evolution in which the hysteresis loop shrinks over time in current control and the points above the threshold voltage change over time in voltage control. (b) V–I measurements at 50 K with data averaged at each step showing symmetrical response to positive and negative current. Panes (c) and (d) show calculated resistance corresponding to the plots above.

Additional data were obtained on the puck-mounted sample, which exhibited a slightly lower resistivity than the 50 W sample but shared the same T_{IMT} and displayed a $R(T)$ curve with a similar shape. The initial resistance in electrical measurements was also marginally lower, but a larger threshold voltage was observed in these measurements (12.5 V at 50 K in figure 3(a) compared to 9 V at 50 K in figure 2(b)).

To examine the impact of ambient temperature, current-controlled V–I curves were measured at various temperatures (figure 3(a)), revealing a decrease in the threshold voltage with increasing temperature. This observation aligns with the initial resistance decreasing as temperature increases (figure 3(c)). V_{th} demonstrated a roughly linear relationship with temperature within the measured range (figure 3(b)), although the NDR region disappeared at 125 K and higher, consistent with the measured IMT temperatures in figure 1(b).

4. Modeling

Previous studies of volatile memristors have often used the phase fraction model to emulate the behavior of VO_2

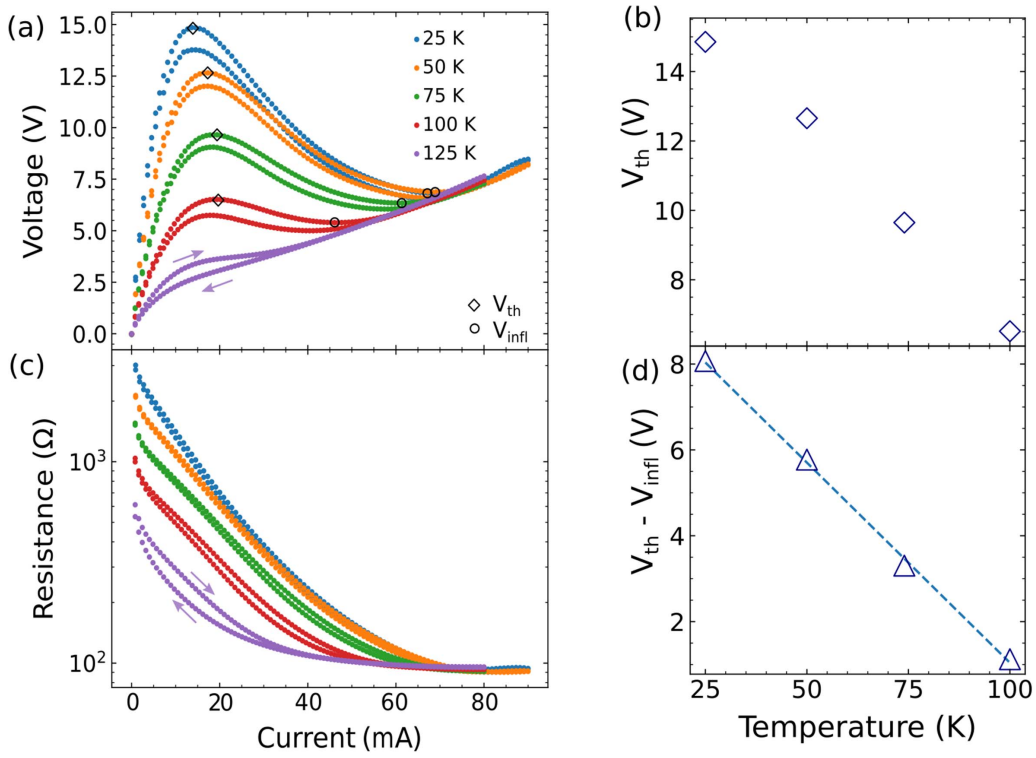

Figure 3. (a) Current-controlled *V*–*I* measurements of sample on resistivity puck taken at various temperatures, (b) calculated resistance for each *V*–*I* curve, (c) threshold voltage (marked in part (a)) vs temperature, and (d) difference between threshold and inflection voltage vs temperature. Dashed line indicates linear fit.

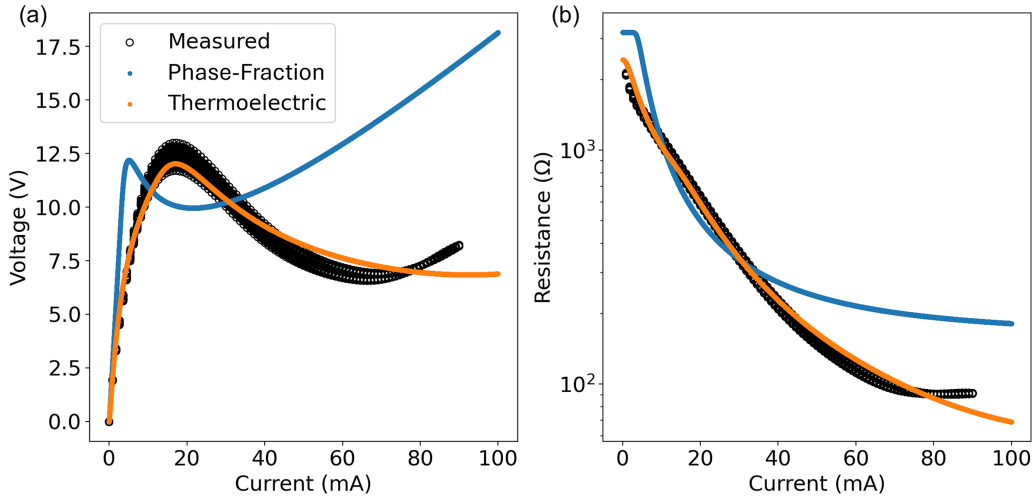

Figure 4. (a) Measured *V*–*I* data (30 W sample, 50 (K) and two models described, (b) resistance calculated from the data.

and NbO_2 devices [15, 19]. In the phase fraction model, the resistivities of the insulating and conductive phases are assumed to be constant and the amount of each phase varies with temperature. In most measurements of VO_2 and NbO_2, the resistance has minimal dependence on temperature away from the IMT temperature, but in our measurements the resistance maintained a large temperature dependence in low temperatures. Thus, extracting a single value for the insulating-phase resistivity of $NdNiO_3$ is not obvious. In the thermoelectric model, the overall device resistivity continuously varies with temperature. In both models, the device temperature increases due to resistive heating and decreases due to passive conduction to the environment. Figure 4 shows an example of measured *V*–*I* data (figure 3(a) 50 K) and the two models manually fit to represent it as closely as possible.

The phase fraction model uses commonly-measured material properties such as heat capacity and thermal conductivity, so characteristic values were chosen based on literature and

measurements. The resistance values at 50 K and 150 K were used for the insulating-phase and metallic-phase resistivities. To better represent the measured *V–I* data, other parameters were manually adjusted, especially geometric values since the conduction path is unknown. These parameters and simulation conditions are shown in the supplemental material.

The thermoelectric model, which defines resistivity as a function of temperature, has also been used for transition metal oxide memristors [1, 9]. These studies used a physics-based model for hopping conduction to describe $R(T)$ for NbO_2 and TiO_2 [1, 9]. Previous studies of $NdNiO_3$ found that $R(T)$ below T_{IMT} is fit best by a combined thermally activated and hopping model [5]. This equation was combined with a logarithmic model for the metallic behavior, where the resistivity increases with temperature but on a smaller scale than the IMT. A linear regression was used to fit the combined model to the measured $R(T)$ curve. Thermal resistivity and thermal capacitance govern the change in temperature in response to applied current. Those parameters were manually fit to the measured *V–I* data.

5. Discussion

The two films studied here had slightly different absolute resistivity values, but similar magnitudes of their IMTs. They also had slightly different out-of-plane lattice parameters. Oxygen vacancies are known to expand the out-of-plane lattice constant in epitaxial oxide films, and could explain the difference in resistivity between the two films, because they act as electron dopants that take up conducting states [11]. While understanding growth parameters is clearly important, the extrinsic value of resistance matters most for device applications, and it can be controlled via device dimensions.

Initial device measurements (figure 2(a)) showed the expected s-type NDR under current control, indicating that the change in resistance under electrical stimulus is most likely phase change due to resistive heating. The resistance evolution is symmetric under both positive and negative applied current (figure 2(d)), as would be expected for the symmetric device structure.

However, the hysteresis loops in the current sweeps in figure 2 were unexpected. In the current-controlled measurement, the points on the increasing and decreasing sweeps move towards each other over time, suggesting that the hysteresis would close for an infinitely slow measurement. In figure 2(b), the slight differences in resistance around 0 mA are also due the thermal transient: the sweep up in positive current occurs after the sweep down from negative current, so residual heat in the device causes a slightly lower initial resistance. The fact that the rate of cooling was slower than the *V–I* measurements, which took 1–2 min, poses a challenge for volatile resistive switching. However, the devices examined here are 1 mm or more in length, and smaller devices would require less heat to switch phase and thus have to dissipate less heat to switch back.

Subsequent measurements with the second sample on the resistivity puck (figure 3(a)) show that the hysteresis loops become smaller on the puck with higher thermal conduction than the chip holder. These measurements highlight the impact of the environment directly around the thin-film device. The rate of cooling could therefore be increased by using substrates with higher thermal conductivity or mesa-isolating vertical devices to limit the active thermal mass.

In the measurements on the resistivity puck, V_{th} is inversely related to temperature, and the initial resistance can also be seen decreasing as temperature increases. V_{infl} varies less with temperature, because the final, metallic-phase resistance is the same in every measurement (figure 3(c)). This results in the peak-to-valley voltage, $V_{th}-V_{infl}$, decreasing linearly with temperature (figure 3(d)). When it crosses zero, there is no longer any NDR in the *V–I* curve.

The fact that these devices operate on a steep slope of $R(T)$ is also reflected in the better fit of the thermoelectric model. In the phase fraction model, the resistance would be constant for small current inputs that provide small amounts of heat, but the material measured here responds with a large change in conductivity for even small increases in temperature (figure 4(b)). Therefore, the thermoelectric model, that uses temperature as an independent variable, can capture the low-current *V–I* behavior more accurately.

The thermal dependence is also potentially useful as an additional variable. Neighboring devices might locally heat a device they are not directly connected to, reducing its threshold voltage. Rather than treating such an effect as thermal noise, it could be used to mimic biological behaviors such as heterosynaptic plasticity. In biological systems, subthreshold stimulus can induce short- and long-term plasticity [8, 18]. In a similar way, thermal stimulus in neighboring switching devices could reduce the threshold for switching on long or short timescales, depending on the rate of cooling in the devices.

6. Conclusions

In conclusion, this study has demonstrated volatile memristive behavior in $NdNiO_3$ that matches the temperature-dependent measurements of the film, indicating the measured electrical behavior is dominated by bulk resistivity effects. While the relative change in resistivity is a specific property of the film that is highly sensitive to growth conditions, the absolute value of resistance can be scaled with the device volume. The resistance can also be adjusted with temperature, perhaps locally within an array of devices, due to the steep slope of decreasing $R(T)$ at low temperatures. This effect is better captured with a thermoelectric model, in contrast to previous work modeling similar IMT materials with the phase-fraction model. Like other studies of IMT memristors, this work shows that $RNiO_3$ devices can demonstrate characteristic volatile behaviors, and are applicable to neuron-like switching devices. Our findings indicate scalable, phase-change-driven behavior that could be significantly scaled to dense arrays of devices for artificial neural network applications.

Data availability statement

All data that support the findings of this study are included within the article (and any supplementary files).

Acknowledgment

This work was authored in part by the National Renewable Energy Laboratory (NREL), operated by Alliance for Sustainable Energy, LLC, for the U.S. Department of Energy (DOE) under Contract No. DE-AC36-08GO28308. This work was supported by the Laboratory Directed Research and Development (LDRD) Program at NREL. The views expressed in the article do not necessarily represent the views of the DOE or the U.S. Government. The U.S. Government retains and the publisher, by accepting the article for publication, acknowledges that the U.S. Government retains a nonexclusive, paid-up, irrevocable, worldwide license to publish or reproduce the published form of this work, or allow others to do so, for U.S. Government purposes. O S acknowledges funding from the Coorstek Fellowship.

ORCID iDs

O D Schneble https://orcid.org/0000-0002-2089-1600
I A Leahy https://orcid.org/0000-0002-4483-1813
J D Zimmerman https://orcid.org/0000-0001-8936-5345
M B Tellekamp https://orcid.org/0000-0003-3535-1831

References

[1] Alexandrov A S, Bratkovsky A M, Bridle B, Savel'ev S E, Strukov D B and Stanley Williams R 2011 Current-controlled negative differential resistance due to Joule heating in TiO_2 *Appl. Phys. Lett.* **99** 202104

[2] Andrews J L, Santos D A, Meyyappan M, Williams R S and Banerjee S 2019 Building brain-inspired logic circuits from dynamically switchable transition-metal oxides *Trends Chem.* **1** 711–26

[3] Brown T D, Kumar S and Williams R S 2022 Physics-based compact modeling of electro-thermal memristors: negative differential resistance, local activity and non-local dynamical bifurcations *Appl. Phys. Rev.* **9** 011308

[4] Brown T D, Bohaichuk S M, Islam M, Kumar S, Pop E and Williams R S 2023 Electro-thermal characterization of dynamical VO_2 memristors via local activity modeling *Adv. Mater.* **35** 2205451

[5] Catalan G, Bowman R M and Gregg J M 2000 Metal-insulator transitions in $NdNiO_3$ thin films *Phys. Rev.* B **62** 7892–900

[6] Catalano S, Gibert M, Fowlie J, Iniguez J, Triscone J-M and Kreisel J 2018 Rare-earth nickelates $RNiO_3$: thin films and heterostructures *Rep. Prog. Phys.* **81** 046501

[7] del Valle J, Rocco R, Domínguez C, Fowlie J, Gariglio S, Rozenberg M J and Triscone J-M 2021 Dynamics of the electrically induced insulator-to-metal transition in rare-earth nickelates *Phys. Rev.* B **104** 165141

[8] Fino E, Deniau J-M and Venance L 2009 Brief subthreshold events can act as Hebbian signals for long-term plasticity *PLoS One* **4** 1–11

[9] Gibson G A *et al* 2016 An accurate locally active memristor model for s-type negative differential resistance in NbO_x *Appl. Phys. Lett.* **108** 023505

[10] Hauser A J, Mikheeev E, Moreno N E, Cain T A, Hwang J, Zhang J Y and Stemmer S 2013 Temperature-dependence of the Hall coefficient of $NdNiO_3$ thin films *Appl. Phys. Lett.* **103** 182105

[11] Kotiuga M *et al* 2019 Carrier localization in perovskite nickelates from oxygen vacancies *Proc. Natl Acad. Sci.* **116** 21 992–21 997

[12] Kumar S, Strachan J P and Williams R S 2017 Chaotic dynamics in nanoscale NbO_2 Mott memristors for analogue computing *Nature* **548** 318–21

[13] Kumar S and Williams R S 2018 Separation of current density and electric field domains caused by nonlinear electronic instabilities *Nat. Commun.* **9** 2030

[14] Pickett M D and Williams R S 2012 Sub-100 fJ and sub-nanosecond thermally-driven threshold switching in niobium oxide crosspoint nanodevices *Nanotechnology* **23** 215202

[15] Pickett M D, Medeiros-Ribeiro G and Williams R S 2013 A scalable neuristor built with Mott memristors *Nat. Mater.* **12** 114–7

[16] Pickett M D, Borghetti J, Yang J J, Medeiros-Ribeiro G and Williams R S 2011 Coexistence of memristance and negative differential resistance in a nanoscale metal-oxide-metal system *Adv. Mater.* **23** 1730–3

[17] Yang J J, Strukov D B and Stewart D R 2013 Memristive devices for computing *Nat. Nanotechnol.* **8** 13–24

[18] Yang Y, Chen B and Lu W D 2015 Memristive physically evolving networks enabling the emulation of heterosynaptic plasticity *Adv. Mater.* **27** 7720–7

[19] Yi W, Tsang K K, Lam S K, Bai X, Crowell J A and Flores E A 2018 Biological plausibility and stochasticity in scalable VO_2 active memristor neurons *Nat. Commun.* **9** 4661